V.F.5 Performance and Durability of Advanced Automotive Fuel Cell Stacks and Systems with Nanostructured Thin Film Catalyst Based Membrane Electrode Assemblies

Rajesh K. Ahluwalia (Primary Contact),
Xiaohua Wang, and J-K Peng
Argonne National Laboratory
9700 South Cass Avenue
Argonne, IL 60439
Phone: (630) 252-5979
Email: walia@anl.gov

DOE Manager: Nancy L. Garland
Phone: (202) 586-5673
Email: Nancy.Garland@ee.doe.gov

Project Start Date: October 1, 2003
Project End Date: Project continuation and direction determined annually by DOE

Overall Objectives

- Develop a validated model for automotive fuel cell systems, and use it to assess the status of the technology.
- Conduct studies to improve performance and packaging, to reduce cost, and to identify key R&D issues.
- Compare and assess alternative configurations and systems for transportation and stationary applications.
- Support DOE U.S. DRIVE automotive fuel cell development efforts.

Fiscal Year (FY) 2016 Objectives

- Quantify the impact of thinner membranes, lower anode Pt loadings, and high-activity de-alloyed nanostructure thin film (NSTF) Pt_3Ni_7 cathode on the performance of automotive stacks and fuel cell systems.
- Understand the durability of NSTF electrode under long potentiostatic holds.
- Extend system analysis to alternate non-NSTF membrane electrode assemblies (MEAs) with conventional Pt/C and advanced Pt alloy/C cathode catalysts.
- Incorporate durability considerations in system analysis.
- Provide modeling support to Eaton's development of Roots air supply system.

Technical Barriers

This project addresses the following technical barriers from the Fuel Cells section of the Hydrogen, Fuel Cells, and Infrastructure Technologies Program Multi-Year Research, Development, and Demonstration Plan:

(A) Durability

(B) Cost

(C) Performance

Technical Targets

This project is conducting system level analyses to address the following DOE 2020 technical targets for automotive fuel cell power systems operating on direct hydrogen.

- Energy efficiency: 60% at 25% of rated power
- Q/DT: 1.45 kW/°C
- Power density: 850 W/L for system, 2,500 W/L for stack
- Specific power: 850 W/kg for system, 2,000 W/kg for stack
- Transient response: 1 s from 10% to 90% of maximum flow
- Start-up time: 30 s from –20°C and 5 s from +20°C ambient temperature
- Precious metal content: 0.125 g/kW_e rated gross power

Accomplishments

- Quantified the sources of 14–20% decrease in power density and \$2.20/kW_e increase in cost due to the heat rejection (Q/DT) constraint.
- Identified the dominant NSTF catalyst degradation mode and determined that the cumulative fluoride release (CFR) must be limited to 0.7 $mg.cm^{-2}$ for 10% performance degradation over 5,000 h.
- Projected 25% increase in power density and 16.8% reduction in stack cost by reducing anode Pt loading to 0.02 mg/cm^2, and replacing $Pt_{68}(CoMn)_{32}$/NSTF with Pt_3Ni_7/NSTF cathode catalyst and 20-mm 835 equivalent weight (EW) membrane with supported 14-mm 725 EW membrane.
- Demonstrated that, compared to a baseline unit, the V250 module (without expander) reduces parasitic

power by 6.4% at full flow (92 g/s) and by 35% at quarter flow (25 g/s).

INTRODUCTION

While different developers are addressing improvements in individual components and subsystems in automotive fuel cell propulsion systems (i.e., cells, stacks, balance-of-plant components), we are using modeling and analysis to address issues of thermal and water management, design-point and part-load operation, and component-, system-, and vehicle-level efficiencies and fuel economies. Such analyses are essential for effective system integration.

APPROACH

Two sets of models are being developed. The GCtool software is a stand-alone code with capabilities for design, off-design, steady state, transient, and constrained optimization analyses of fuel cell systems (FCS). A companion code, GCtool-ENG, has an alternative set of models with a built-in procedure for translation to the MATLAB Simulink platform commonly used in vehicle simulation codes, such as Autonomie.

RESULTS

We collaborated with 3M in designing tests on 5-cm^2 active-area differential cells and analyzing the data to model the performance of full-area (>250 cm^2) cells with 3M's state-of-the-art binary dealloyed NSTF catalyst with Pt/C cathode interlayer [1]. The following are the details of the MEA selected for this study.

- Ternary Anode: $Pt_{68}(CoMn)_{32}$, 0.019 mg_{Pt}/cm^2
- Binary Cathode: Pt_3Ni_7/NSTF, dealloyed (Johns Hopkins University chemistry), 0.096 mg_{Pt}/cm^2
- Membrane: 3M-S (supported) 725 EW) perfluorosulfonic acid stabilized with chemical additive, 14 mm
- Anode Gas Diffusion Layer (GDL): 3M "X3" (experimental backing, 3M hydrophobization)
- Cathode GDL: 3M 2979
- Cathode Interlayer: 3M Type "B", 0.016 mg_{Pt}/cm^2

For reproducibility of data, the test campaign included three thermal conditioning cycles (TCs) in normal and reverse flow before each test series and 1 TC before each polarization curve. Test series were designed to obtain performance data over a wide range of pressure (P: 1–3 bar), temperature (T: 45–90°C), O_2 mole fraction ($X(O_2)$: 1–21%, 100%;), anode relative humidity (RH(a): 30–100%) and cathode relative humidity (RH(c): 30–150%), all at constant hydrogen ($Q(H_2)$: 1 slpm) and air (Q(air): 3 slpm) flow rates. Changes in high frequency resistance, H_2 crossover, mass activity, electrochemical surface area (ECSA), and short resistance were monitored. Over ~735 h actual test time, the ECSA decreased by ~25% from 22.9 to 17.2 m^2/g. Figure 1a shows the variability in polarization curve at the reference conditions that were visited multiple times during the course of the campaign. We did not observe any significant systematic degradation and have classified the polarization curves in two groups, high performance (HIP) and representative performance (REP).

We estimated the oxygen reduction reaction (ORR) kinetic parameters from internal resistance and crossover corrected cell voltages at low current densities in H_2/O_2 and H_2/air (see Figures 1b, 1c, and 1d). The modeled mass activity of binary Pt_3Ni_7/NSTF with cathode interlayer was compared with the data for two other NSTF catalysts analyzed in earlier works [2,3]. In general, the modeled mass activities of all three catalyst systems are consistent with the data obtained using the 3M standard protocol. Compared to the baseline ternary $Pt_{68}(CoMn)_{32}$/NSTF catalyst, the mass activity of binary d-Pt_3Ni_7/NSTF catalyst with cathode interlayer is 78–144% higher.

We determined the limiting current density (i_L) and correlated mass transfer overpotential (h_m) with reduced the current density (i/i_L). For convenience, we defined i_L as the current density at which h_m = 300 mV. In our terminology, h_m includes any internal resistance drop in the electrode. We also determined relationships between h_m (and i_L) and all operating variables: P, T, $X(O_2)$, RH(a), RH(c), i/i_L. Figures 1e and 1f are illustrative examples of this relationship for one variable, i.e., pressure.

Work is underway to calibrate the performance model developed using differential cell data with 50-cm^2 cell data for finite cathode/anode stoichiometries and operating temperatures needed to satisfy the Q/DT constraint. The preliminary results indicate that 3M's best-of-class (BOC) 50-cm^2 cell data are closer to the modeled results without mass transfer overpotentials. There is a parallel ongoing effort to replicate 3M's BOC performance with identical cells and conditioning procedures. In the future, we also hope to validate our model with data from full-area short stack being built.

We integrated the cell model in our FCS analysis code and conducted a study to project the beginning of life performance of FCS with d-Pt_3Ni_7/NSTF catalyst and cathode interlayer, subject to Q/DT constraint [3], The MEAs in this study have 0.131 mg/cm^2 total Pt loading and 725 EW, 14 mm 3M-S membrane. At optimal conditions, the optimal power density is determined by high frequency resistance and ORR activity rather than mass transfer overpotentials. The projected cost ($1,500/tr-oz Pt price) and Pt content are

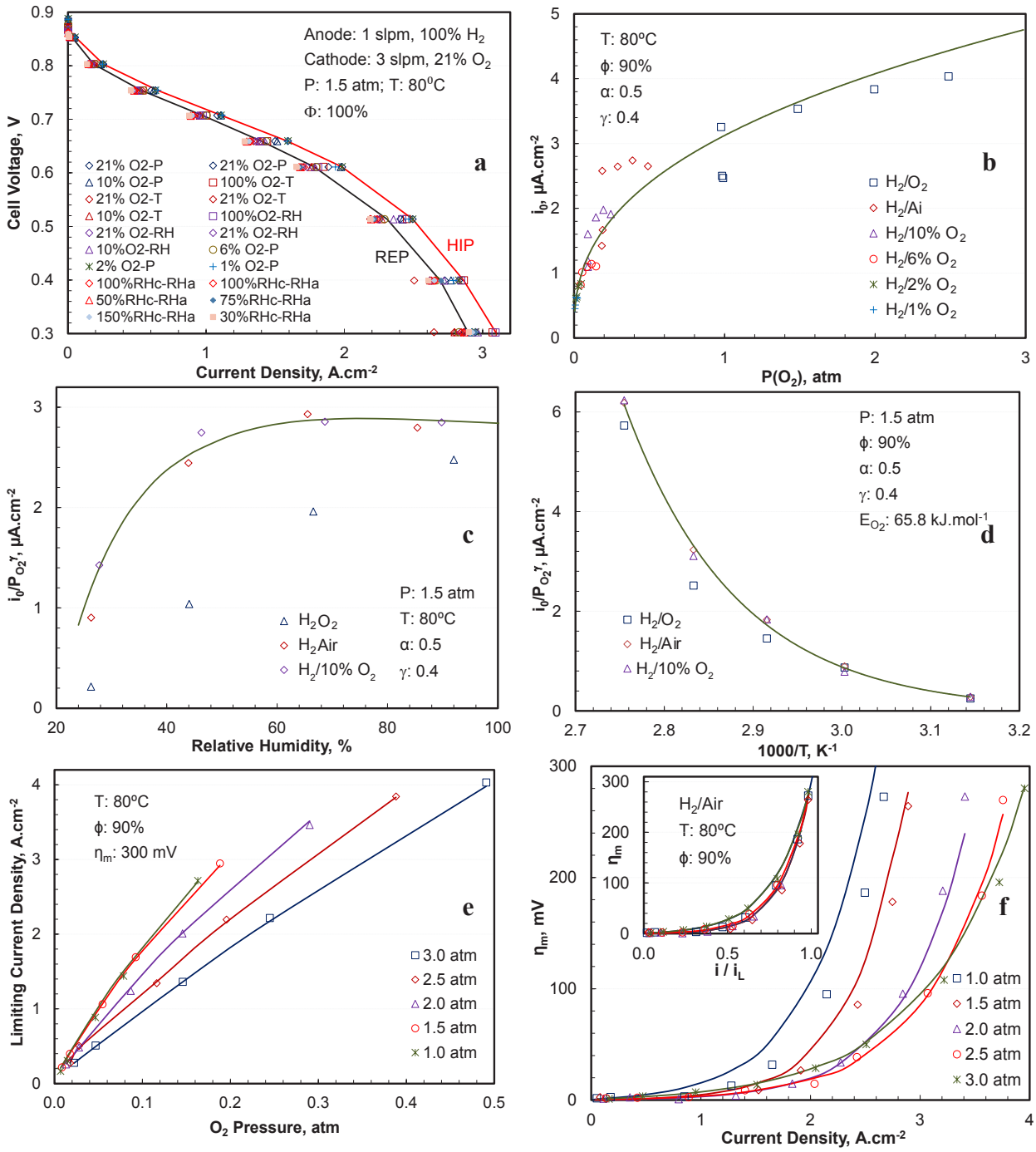

FIGURE 1. Development of performance model using differential cell data for MEA with d-Pt_3Ni_7 NSTF catalyst with cathode interlayer. Equation for ORR kinetics: $i + i_x = i_{0r} P_{O2}^{\gamma} \phi^{\beta} e^{\frac{E_{O2}}{R}(\frac{1}{T}-\frac{1}{T_r})} e^{\frac{\alpha n F}{RT}\eta}$. Reproducibility of test data for standard conditions; (b) ORR kinetics: P(O_2) dependence; (c) ORR kinetics: RH dependence; (d) ORR kinetics: T dependence; (e) Limiting current density correlation; (f) Mass transfer overpotential correlation. Solid lines are model results.

$48.4–48.7/$kW_e$ at 2.2–2.5 atm, and 0.152–0.155 g-Pt/kW_e at 2.5–3.0 atm stack inlet pressure, see Figures 2a and 2b.

Figures 2c, 2d, and Table 1 compare the cost and performance of fuel cell systems with different NSTF catalysts and membranes. The 2015 reference FCS includes ternary catalyst MEA and 20 mm, 835 EW membrane without mechanical reinforcement [4]. The 2016 reference FCS includes binary NSTF catalyst with Pt/C cathode

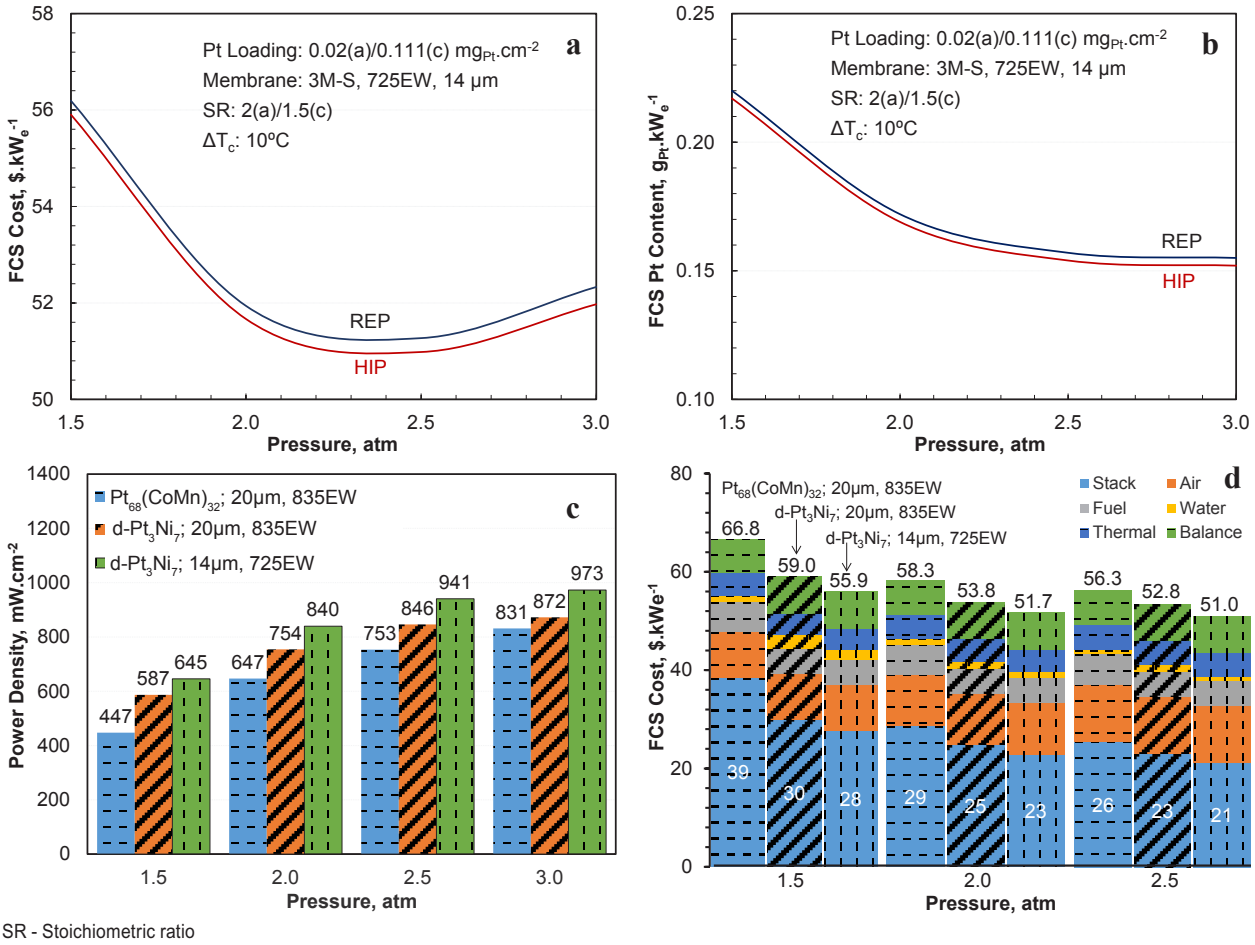

SR - Stoichiometric ratio

FIGURE 2. Projected performance and cost of automotive fuel cell systems with NSTF catalyst based MEAs. (a) Minimum FCS cost at different stack inlet pressures; (b) FCS Pt content at optimum conditions; (c) Stack power density for different NSTF MEAs; (d) FCS cost for different NSTF MEAs

TABLE 1. Summary Performance of Stacks with Different NSTF Catalysts and Membranes

Cathode / Anode Catalyst	Membrane	Cathode / Anode Pt Loading	Power Density (2.5 atm)	Stack Cost (2.5 atm)
C: $Pt_{68}(CoMn)_{32}$	20 μm, 835 EW	0.1 mg/cm^2	753 mW/cm^2	25.69 $/kW$_e$
A: $Pt_{68}(CoMn)_{32}$		0.05 mg/cm^2		
C: d-Pt_3Ni_7 + Cathode Interlayer	20 μm, 835 EW	0.095 + 0.016 (CI) mg/cm^2	+12.3%	-10.0%
A: $Pt_{68}(CoMn)_{32}$		0.02 mg/cm^2		
C: d-Pt_3Ni_7 + Cathode Interlayer	14 μm (S), 725 EW	0.095 + 0.016 (CI) mg/cm^2	+25.0%	-16.8%
A: $Pt_{68}(CoMn)_{32}$		0.02 mg/cm^2		

interlayer and mechanically reinforced 14 mm, 725 EW membrane. For better understanding of results, we included an FCS with binary NSTF catalyst and Pt/C cathode interlayer but 20 mm, 835 EW membrane as in 2015 FCS. Compared to the 2015 reference FCS, the 2016 FCS has 25% higher stack power density: 12.3% due to higher ORR activity and 12.7% due to thinner membrane. It also has 16.8% lower stack cost: 10% due to higher ORR activity and 6.8% due to thinner membrane. The projected performance and cost of 2016 FCS are 973 mW/cm^2 stack power density,

0.152 g/kW$_e$ Pt content, and 48.40 $/kW$_e$ system cost at high volume manufacturing.

Durability of MEAs with NSTF Catalysts

We have been collaborating with 3M to develop a test protocol for determining the stability of the baseline ternary NSTF catalyst under potentiostatic conditions [5]. The protocol consists of repeatedly degrading the cell for 10 h at constant potential with periodic F^- collection and partial reconditioning with 1 TC cycle. Every 20 h of degradation, polarization curves are taken in H_2/air. Every 40–80 h of degradation, the cell is reconditioned more fully with 3 TC cycles and data are obtained to measure the cathode ORR activity, cathode ECSA, H_2 crossover, shorting resistance, and cell polarization in H_2/air. The tests were run on 50-cm^2 cells with quad serpentine flow fields and ternary catalysts with 0.05 mg/cm^2 Pt loading on anode and 0.15 mg/cm^2 Pt loading on cathode. The cells used 3M, 825 EW, membrane that was 20 mm thick. The membrane was chemically stabilized with an anti-oxidant additive but was not mechanically supported.

Figures 3a and 3b present voltage degradation determined from the polarization curves for three current densities representing near open-circuit condition (0.032 A/cm^2), kinetic region (0.32 A/cm^2), and the region where the mass transfer overpotentials may become important (1 A/cm^2). The voltage degradation rates are comparable at 0.032 A/cm^2 and 0.32 A/cm^2 indicating that the underlying mechanism may be related to the slowdown of ORR kinetics at low current densities. The voltage degradation rates are much larger at 1 A/cm^2 suggesting that mass transfer in the MEA is also impeded with exposure time. The data quantitatively confirms that the voltage degradation rates are accelerated at lower hold potentials and higher exposure temperatures.

Figures 3c and 3d present the fluoride emission rate (FER) measured by ion chromatography of the collected water samples. F^- concentrations in the water samples were

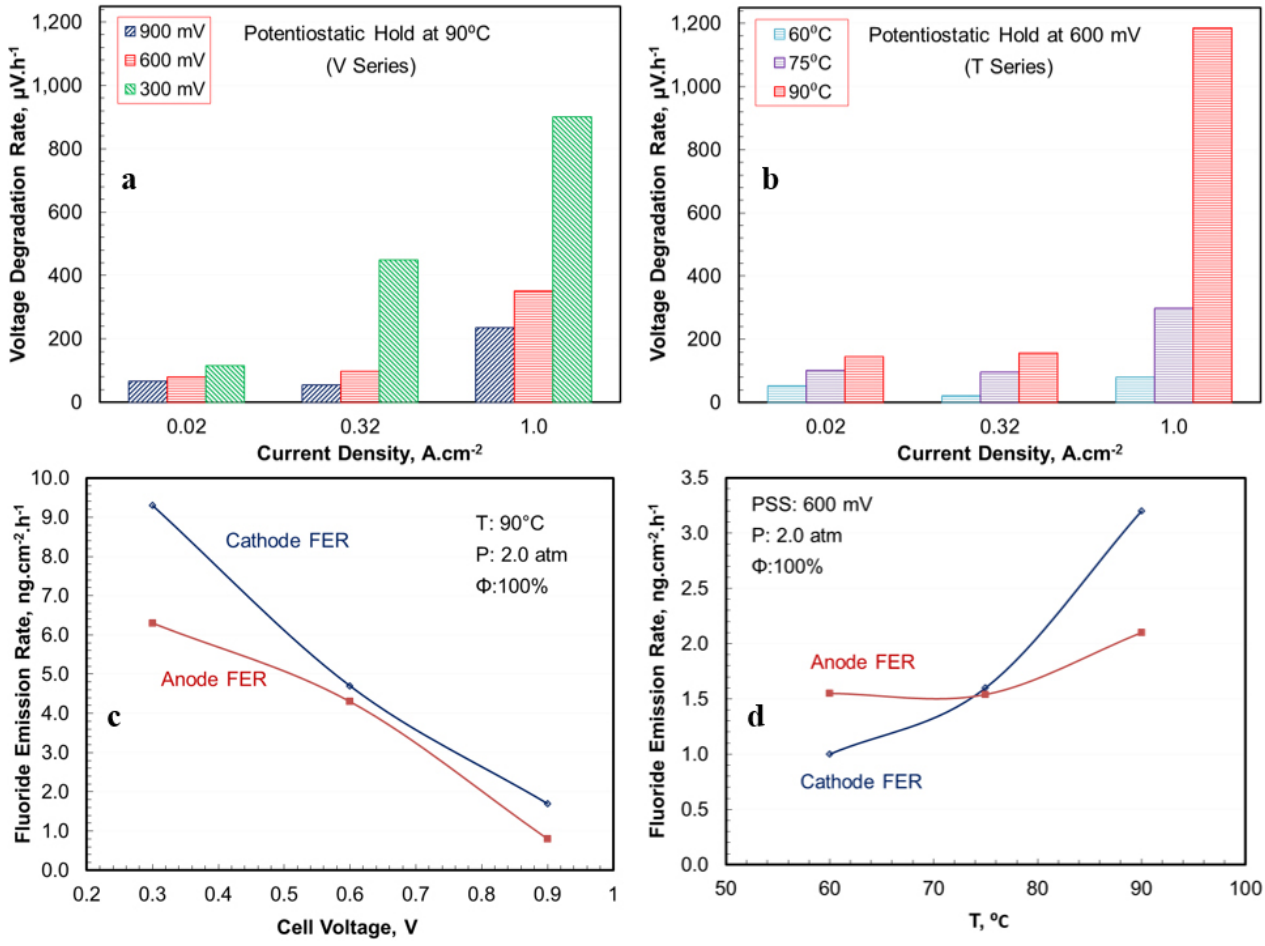

PSS – Potentiostatic scan

FIGURE 3. Durability of NSTF catalyst and MEA under long potentiostatic holds at 0.3–0.9 V. (a) Voltage degradation at different hold potentials; (b) Voltage degradation at different temperatures; (c) FER at different hold potentials; (d) FER at different temperatures.

very low, 20 ppb or less. Although the concentrations were similar, F^- generation rate increases with decreasing hold potential (i.e., increasing current density) due to higher effluent water flow rate (production + supplied). The measured FERs are similar but higher on cathode than on anode for all hold potentials, suggesting that FER measured in cathode effluent was produced locally in cathode. The trend of measured cathode FER increasing with decreasing cell voltage is consistent with the observed dependence of H_2O_2 production on potential in rotating ring disk electrode tests [6]. The measured anode FER correlates with the cell voltage rather than the anode potential. Rotating ring disk electrode experiments in a hydrogen environment have shown that H_2O_2 generation decreases as the anode potential is raised. For these reasons, it is unlikely that the measured F^- in anode effluent water was due to H_2O_2 produced locally in the anode by the reaction of O_2 crossing over from the cathode ($2H^+ + O_2 + 2e^- = H_2O_2$). Further work is needed to determine whether FER on cathode and anode are related and if F^- detected in anode water was actually produced in the cathode and permeated through the membrane.

We used the data for F^- concentration in effluent cathode water samples obtained during V-series and T-series to develop the following empirical correlation for cathode FER (N_F, mg/cm^2.h) as a function of cell potential (E, V) and exposure temperature (T, K).

Figure 4a presents the measured loss in surface enhancement factor (SEF, cm^2-Pt/cm^2-planar), that is the product of the ECSA (cm^2-Pt/mg-Pt) and the Pt loading (L_{Pt}, mg-Pt/cm^2). It indicates that the higher the exposure temperature the greater is the rate of loss of SEF at 600 mV hold potential, but the maximum loss is limited to about 30% to 40% at 60 A/cm^2 90°C. SEF loss appears to be self-limiting and ceases when the whiskerettes dissolve and disappear. Previous studies showed similar SEF loss when the NSTF catalyst was subjected to 30,000 triangle potential cycles in H_2/N_2 (cyclic voltammetry) and H_2/air

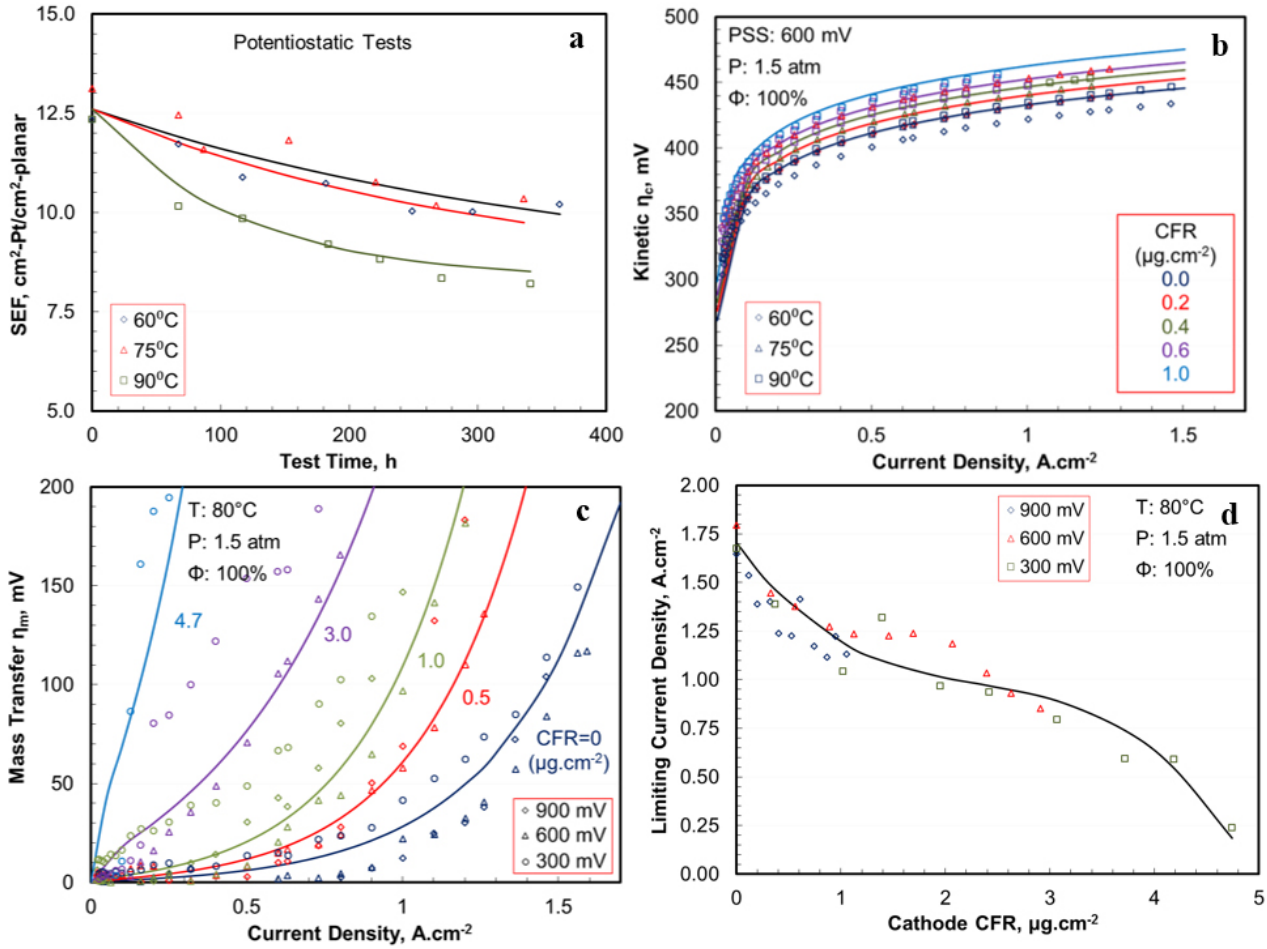

FIGURE 4. Development of NSTF MEA durability model using measured degradation in ECSA, ORR kinetics, limiting current density and O_2 mass transfer. (a) Loss in electrochemical surface area; (b) Increase in ORR kinetic loss; (c) Increase in mass transfer overpotential; (d) Reduction in limiting current density. Solid lines are model results.

(dynamic load cycles) with 0.6 V lower potential limit, 0.9 to 1.0 V upper potential limit, and 50 mV scan rate at 80°C and 100% RH [7]. These results may be compared with 60–80% SEF loss from 3–5 nm diameter or smaller nano-Pt particles dispersed on high-surface area carbon support (>60–80 m^2/g-Pt ECSA), when subjected to cyclic potentials. The NSTF ternary catalyst is supported on 27±7 nm x 55±12 nm rectangular lath-like 0.6–2μm length organic whiskers, has much smaller initial ECSA (A_{Pt}^0), <10 m^2/g-Pt, but its ECSA is more stable. Whereas, the dispersed nano-Pt/C catalysts lose ECSA as Pt dissolves and the particles coarsen due to the Ostwald ripening mechanism and coalescence and sintering, the NSTF catalyst loses ECSA because of the dissolution of Pt whiskerettes and the resulting reduction in surface roughness.

We determined the kinetic parameters from the measured polarization curves at low current densities where the mass transfer overpotentials are negligible. Figure 4b presents the estimated kinetic overpotentials as a function of current density and CFR for the six tests. The solid linear lines in Figure 4b, representing the least-square fit of the data, are nearly parallel, implying that there are only small changes in the Tafel slope with ageing at potentiostatic hold and the symmetry factor has remained constant. The linear offset in parallel lines is a measure of the changes in the exchange current density and ECSA. We have used these data to estimate the changes in the exchange current density, (μA/cm^2-Pt), with ageing, and found a strong and explicit correlation between and CFR, the cumulative fluoride release (N_F, mg/cm^2). The dependence of on hold potential and exposure temperature, however, is implicit since and, therefore, N_F is a function of E and T.

We determined the mass transfer overpotentials (η_m) from the measured polarization curves and the derived ORR kinetic parameters. As defined, η_m includes any Ohmic drops (iR_Ω^c) in the electrode layer, which may be small since the electrode is extremely thin, <0.5 mm. Figure 4c quantifies the increase in mass transfer overpotentials with ageing; this increaseis larger at lower hold potentials and higher exposure temperatures. The effect of ageing on is related to the diminished O_2 diffusion through the MEA. We suggest that the observed increase in after long potentiostatic hold is due to the degradation of the catalyst layer rather than due to changes in the GDL or the gas flow field.

We developed a correlation for the limiting current density, defined for convenience as the reference current density (i_L) at which the mass transfer overpotential (h_m) equals 200 mV. Figure 4d shows that is strongly correlated with N_F, and decreases as more fluoride is released at the cathode. Since the absolute amount of F^- release is small, the decrease in is likely related to contamination of the NSTF catalyst (~15 cm^2-Pt/cm^2 planar area) with membrane decomposition products rather than degradation of GDL (>30 cm^2/cm^2 surface area) or the gas channel. One plausible mechanism by which contaminants in small quantities can affect O_2 mass transport in NSTF catalysts is by modifying its wetting characteristic. Compared to the dispersed Pt/C catalysts, the NSTF catalysts are known to be more susceptible to poisoning by external impurities because of their smaller surface area. We developed a correlation for mass transfer overpotential (h_m in mV) assuming that it is only a function of . Implicitly, h_m is also a function of the hold potential and the exposure temperature since and N_F depend on these variables.

The current automotive targets specify 5,000 h lifetime with an allowance for 10% voltage degradation at rated power. Assuming 0.66–0.7 V cell voltage and 1–1.5 A/cm^2 at rated power, these specifications translate to 66–70 mV allowable voltage loss at rated power over lifetime, or 13–14 mV/h average degradation rate. As a comparison, the measured voltage degradation rate corresponding to 1 A/cm^2 varies for the experimental MEA varies between 200–900 mV/h at 300–900 mV hold potential (90°C exposure temperature) and 80–1,200 mV/h at 60 A/cm^2 90°C exposure temperature (600 mV hold potential). The actual degradation rate depends on the duty cycle and can be evaluated using the data and correlations presented in this work. However, the necessity to operate at temperatures below 60°C while avoiding extended excursions at temperatures above 90°C is quite apparent.

Independent of the duty cycle, we can make some observations about the requisite membrane stability. Since our data showed only small changes in the high frequency resistance, hydrogen crossover and shorting resistance, we conclude that the voltage loss with ageing is mostly due to degradation in ORR kinetics and O_2 mass transport. The allowable N_F corresponding to $Dh_c + Dh_m$ = 70 mV leads to an estimate of N_F = 0.7 mg/cm^2 which is slightly less stringent than the allowable N_F (0.5 mg/cm^2) for Dh_m = 35 mV.

CONCLUSIONS AND FUTURE DIRECTIONS

We determined the ORR kinetic parameters from IR and crossover corrected cell voltages at low current densities in H_2/O_2 and H_2/air. Compared to the baseline ternary $Pt_{68}(CoMn)_{32}$/NSTF catalyst, the mass activity of binary d-Pt_3Ni_7/NSTF catalyst with cathode interlayer is 78–144% higher.

We determined the performance and cost of a reference 2016 automotive FCS that includes a stack with binary NSTF catalyst with Pt/C cathode interlayer and mechanically reinforced 14 mm, 725 EW, reinforced membrane. Compared to the 2015 reference FCS that includes a ternary catalyst and 20 mm, 835 EW, unsupported membrane, the 2016 FCS has 25% higher stack power density: 12.3% due to higher ORR activity and 12.7% due to thinner membrane. It also has 16.8% lower stack cost: 10% due to higher ORR activity and 6.8% due to thinner membrane. The projected performance

and cost of 2016 FCS are 973 mW/cm^2 stack power density, 0.152 g/kW$_e$ Pt content, and \$48.40/kW$_e$ system cost at high volume manufacturing.

We have conducted tests (3M collaboration) and developed a model for NSTF catalyst durability under long potentiostatic hold. The model and data show the mechanisms of degradation of ECSA, kinetic activity and O_2 mass transfer and their relationship with fluoride release from membrane. We project that the target of less than 10% lifetime performance degradation can be achieved by restricting CFR to 0.7 mg/cm^2.

FY 2016 PUBLICATIONS/PRESENTATIONS

1. R.K. Ahluwalia, X. Wang, W.B. Johnson, F. Berg, and D. Kadylak, "Performance of a Cross-Flow Humidifier with a High Flux Water Vapor Transport Membrane," Journal of Power Sources, Vol. 291, pp. 225–238, 2015.

2. R.K. Ahluwalia, X. Wang, and A.J. Steinbach, "Performance of Advanced Automotive Fuel Cell Systems with Heat Rejection Constraint," Journal of Power Sources, Vol. 309, pp. 178–191, 2016.

3. R.K. Ahluwalia, X. Wang, and J-K Peng "Fuel Cells Systems Analysis," U.S. DRIVE Fuel Cell Tech Team Meeting, Southfield, MI, July 15, 2015.

4. R.L. Borup, R. Mukundan, Dusan Spernjak, D. Langlois, R. Ahluwalia, D.D. Papadias, Karren More, and Steve Grot, "Carbon Corrosion in PEM Fuel Cells During Drive Cycle Operation," 228th ECS Meeting, Phoenix, AZ, Oct. 11–15, 2015.

5. R.K. Ahluwalia, D.D. Papadias, R.L. Borup, R. Mukundan, and D. Spernjak, "Mechanism and Kinetics of Carbon Corrosion in Polymer Electrolyte Fuel Cells during Drive Cycles," 228th ECS Meeting, Phoenix, AZ, Oct. 11–15, 2015.

6. R.K. Ahluwalia, and N. Garland, "Report from the Annexes: Annex 34," IEA AFC ExCo 51st Meeting, Phoenix, AZ, Oct. 15–16, 2015.

7. Rajesh Ahluwalia and Sunita Satyapal, "U.S. Department of Energy Hydrogen and Fuel Cells Program," Eco-Mobility 2025Plus, Vienna, Austria, November 9–10, 2015.

8. R.K. Ahluwalia, D.D. Papadias, J.K. Thompson, H.M. Meyer III, M.P. Brady H. Wang, J.A. Turner, R. Mukundan, and R. Borup, "Performance Requirements of Bipolar Plates for Automotive Fuel Cells," IEA Annex 34 Meeting, Vienna, Austria, Nov. 11, 2015.

REFERENCES

1. A.J. Steinbach, "High Performance, Durable, Low Cost Membrane Electrode Assemblies for Transportation Applications," DOE Hydrogen and Fuel Cells Program, FY 2015 Annual Progress Report (2015) V-73 – V-79.

2. R.K. Ahluwalia, X. Wang, A. Lajunen, A.J. Steinbach, S.M. Hendricks, M.J. Kurkowski, and M.K. Debe, "Kinetics of Oxygen Reduction Reaction on Nanostructured Thin-Film Platinum Alloy Catalyst," J. Power Sources 215 (2012) 7788.

3. R.K. Ahluwalia, X. Wang, and A.J. Steinbach, "Performance of Advanced Automotive Fuel Cell Systems with Heat Rejection Constraint," J. Power Sources 309 (2016) 178–191.

4. R.K. Ahluwalia, X. Wang, and J-K Peng, "Performance and Durability of Advanced Automotive Fuel Cell Stacks and Systems," DOE Hydrogen and Fuel Cells Program, FY 2015 Annual Progress Report (2015) V-133 – V-140.

5. A. Kongkanand, J. Zhang, Z. Liu, Y-H Lai, P. Sinha, E.L. Thompson, and R. Makharia, "Degradation of PEMFC observed on NSTF electrodes," J. Electrochem. Soc. 161 (2013) F291–F304.

6. V.A. Sethuraman, J.W. Weidner, A.T. Haug, S. Motupally, and L.V. Protsailo, "Hydrogen Peroxide Formation Rates in a PEMFC Anode and Cathode: Effect of Humidity and Temperature," J. Electrochem Soc., 155 (1) (2008) B50–B57.

7. M.K. Debe, "Tutorial on the Fundamental Characteristics and Practical Properties of Nanostructured Thin Film (NSTF) Catalysts," J. Electrochem. Soc. 160 (6) (2013) F522–F534.